1 **Genetic and molecular mechanism for distinct clinical**

2 **phenotypes conveyed by allelic truncating mutations**

3 **implicated in *FBN1***

4

5 **Mao Lin[a,b*], Zhenlei Liu[c,d*], Gang Liu[a,c], Sen Zhao[a,c], Chao Li[e], Weisheng**

6 **Chen[a,b], Zeynep Coban Akdemir[f], Jiachen Lin[a,b], Xiaofei Song[f], Shengru**

7 **Wang[a,c], Qiming Xu[c], Yanxue Zhao[a], Lianlei Wang[a,b], Yuanqiang Zhang[a,b],**

8 **Zihui Yan[a,b], Sen Liu[a,c], Jiaqi Liu[c,g], Yixin Chen[h], Xu Yang[a], Tianshu Sun[i],**

9 **Xin-Zhuang Yang[i], Yuchen Niu[i], Xiaoxin Li[i], Wesley You[j], Bintao Qiu[i], Chen**

10 **Ding[e], Pengfei Liu[f,k], Shuyang Zhang[c,l], Claudia M. B. Carvalho[f], Jennifer E.**

11 **Posey[f], Guixing Qiu[a,c,m], James R. Lupski[f,n,o,p], Zhihong Wu[c,i,m#], Jianguo**

12 **Zhang[a,c,m#], Nan Wu[a,c,f,m#] , on behalf of the Deciphering Disorders Involving**

13 **Scoliosis and COmorbidities (DISCO) study**

14 [a] *Department of Orthopedic Surgery, Peking Union Medical College Hospital,*

15 *Peking Union Medical College and Chinese Academy of Medical Sciences, Beijing*

16 *100730, China*

17 [b] *Graduate School of Peking Union Medical College, Chinese Academy of Medical*

18 *Sciences, Beijing 100005, China*

19 [c] *Beijing Key Laboratory for Genetic Research of Skeletal Deformity, Beijing 100730,*

20 *China*

21 [d] *Department of Neurosurgery, Xuanwu Hospital, Capital Medical University,*

22 *Beijing 100053, China*

23 [e] *College of Life and Health Sciences, Northeastern University, ShenYang, LiaoNing,*

24 *110819, China*

25 [f] *Department of Molecular and Human Genetics, Baylor College of Medicine,*

26 *Houston, TX 77030, USA*

27 [g] *Department of Breast Surgical Oncology, National Cancer Center /National*

28 *Clinical Research Center for Cancer/Cancer Hospital, Chinese Academy of Medical*

29 *Sciences and Peking Union Medical College, Beijing 100021, China*

30 [h]*Department of Cardiovascular Surgery, Fuwai Hospital, National Center for*

31 *Cardiovascular Diseases, Chinese Academy of Medical Sciences and Peking Union*

32 *Medical College, Beijing 100073, China*

33 [i] *Medical Research Center & Department of Central Laboratory, Peking Union*

34 *Medical College Hospital, Peking Union Medical College and Chinese Academy of*

35 *Medical Sciences, Beijing 100730, China*

36 [j] *Amherst College, 220 South Pleasant Street, Amherst, MA 01002, USA*

37 [k] *Baylor Genetics Laboratory, Houston, Texas 77021, USA*

38 [l] *Department of Cardiology, Peking Union Medical College Hospital, Peking Union*

39   *Medical College and Chinese Academy of Medical Sciences, No. 1 Shuaifuyuan,*

40   *Beijing 100730, China*

41   [m] *Medical Research Center of Orthopedics, Chinese Academy of Medical Sciences,*

42   *Beijing 100730, China*

43   [n] *Departments of Pediatrics, Baylor College of Medicine, Houston, Texas 77030,*

44   *USA*

45   [o] *Texas Children's Hospital, Houston, Texas 77030, USA*

46   [p] *Human Genome Sequencing Center, Baylor College of Medicine, Houston 77030,*

47   *Texas, USA*

48

49   [#] Corresponding authors:

50   Nan Wu, MD, E-mail: dr.wunan@pumch.cn;

51   Jianguo Zhang MD, E-mail: jgzhang_pumch@yahoo.com;

52   Zhihong Wu, MD, E-mail: orthoscience@126.com.

53

54   *These authors have contributed equally to this study

55

56

Abstract

58 The molecular and genetic mechanisms by which different single nucleotide

59 variant (SNV) alleles in specific genes, or at the same genetic locus, bring about

60 distinct disease phenotypes often remain unclear. Allelic truncating mutations of

61 *fibrillin-1(FBN1)* cause either classical Marfan syndrome (MFS) or a more severe

62 phenotype associated with Marfanoid-progeroid-lipodystrophy syndrome (MPLS). A

63 total of three Marfan syndrome/Marfanoid patients (2 singletons and 1

64 parent-offspring trio) were recruited. Targeted next-generation sequencing was

65 performed on all the participants. We analyzed the molecular diagnosis, patient

66 clinical features, and the potential molecular mechanism involved in the MPLS

67 subject in our cohort. We investigated a small cohort, consisting of two classical MFS

68 and one MPLS patient from China, whose clinical presentation included scoliosis

69 potentially requiring surgical intervention. We provide evidence that most nonsense

70 and frameshift mutations lead to *FBN1* null alleles due to mutant mRNA transcript

71 degradation. In contrast, the more severe disease phenotype, MPLS, is caused by

72 mutant mRNAs that are predicted to escape the nonsense mediated decay (NMD)

73 surveillance pathway, making a mutant protein that exerts a dominant negative

74 interference effect to *FBN1* thus generating a gain-of-function (GoF) rather than a

75 loss-of-function (LoF) allele as in MFS. Overall, we provide direct evidence that a

76 dominant negative interaction of *FBN1* potentially explains the distinct clinical

77 phenotype in MPLS patients through genetic and functional analysis of the first

78 Chinese patient with MPLS. Moreover, our study expands the mutation spectrum of

79 *FBN1* and highlights the potential molecular mechanism for MPLS patients.

80 **Keywords**

81 *FBN1*, Marfan syndrome (MFS), Marfanoid-progeroid-lipodystrophy syndrome

82 (MPLS), Targeted next-generation sequencing, Dominant negative mechanism

83

84

85

86   Marfan syndrome (MFS; MIM: #154700) refers to a heritable autosomal dominant

87 disease trait of fibrous connective tissue due to heterozygous mutations in the

88 fibrillin-1 gene (*FBN1*; 134797) on chromosome 15q21. The cardinal phenotypic

89 features allowing for clinical diagnosis primarily occur in the skeletal, ocular, and

90 cardiovascular systems (DIETZ 2015). MFS is manifest by clinical features/findings

91 involving the skeletal (tall stature, disproportionately long limbs and digits

92 [arachnodactyly], anterior chest wall deformity, mild to moderate joint laxity and

93 frequent spinal deformity [especially scoliosis], cardiovascular (increased risk for

94 aortic root dilation and/or dissection), and ocular (*ectopia lentis*) systems (LOEYS *et al.*

95 2010). Marfanoid-progeroid-lipodystrophy syndrome (MPLS; MIM: #616914) is a

96 more recently-clarified fibrillinopathy, and also a complex disease characterized by

97 accelerated aging and postnatal lipodystrophy, poor postnatal weight gain and

98 characteristic dysmorphic facial features that have very rarely been clinically

99 recognized and reported (GOLDBLATT *et al.* 2011; PASSARGE *et al.* 2016). Recent

100 studies have implicated a potential hormone, named asprosin, encoded by the *FBN1*

101 locus as a mediator of the lipodystrophy phenotype (ROMERE *et al.* 2016;

102 DUERRSCHMID *et al.* 2017). All previously reported MPLS individuals consistently

103 harbor heterozygous truncating mutations in exon 64, which leads to premature stop

104   codons in the C-terminal domain of *FBN1* (GOLDBLATT *et al.* 2011; SONG *et al.* 2012;

105   GARG AND XING 2014; JACQUINET *et al.* 2014; PASSARGE *et al.* 2016; ROMERE *et al.*

106   2016).

107   In this study, we present clinical and genetic, genomic and molecular data from

108   three unrelated subjects with Marfan/Marfanoid syndrome, including the first case of

109   clinically recognized MPLS in the Chinese population. The potential effects of

110   truncating mutations of *FBN1* which are implicated in MPLS subjects conveying

111   distinct dominant negative alleles and clinically distinguishable autosomal dominant

112   (AD) disease traits were ascertained with functional assays.

113   **Materials and methods**

114   **Participant recruitment and Sample preparation**

115   A total of three Marfan syndrome/Marfanoid patients (2 singletons and 1

116   parent-offspring trio) were consecutively recruited through the Deciphering Disorders

117   Involving Scoliosis & Comorbidities (DISCO) project (www.discostudy.org) at

118   Peking Union Medical College Hospital (PUMCH). Written informed consent was

119   provided by patients or their parents. Peripheral blood samples were extracted from

120   affected probands and corresponding unaffected parents if available. Genomic DNA

121   was extracted with the QIAamp DNA Blood Mini Kit (QIAGEN, Germany) according

122   to the manufacturer's instructions.

123   **Targeted next-generation sequencing, Variant processing, filtering and**

124   **annotation**

125   To establish an NGS panel maximally covering known genes implicated in the

126   cause of Mendelian diseases with vertebral malformation phenotypes, we performed a

127   systematic literature and database search for congenital scoliosis (CS) related disease.

128   After manual review, a total of 344 genes were found, corresponding to 457 CS related

129   monogenic phenotypes. Also included was an additional set of 220 genes whose

130   protein products are involved in the pathways related to vertebral development or in

131   which pathogenic variant alleles have been reported in association with CS

132   phenotypes in animal models, but not yet linked to human diseases with CS

133   phenotypes. The target panel set comprises 564 genes, 6458 exons and flanking 30bp

134   regions, and 2.97 Mb in total genomic size. DNA Probes for target capture were

135   designed and purchased from NimbleGen (Roche, Switzerland)

136   (https://design.nimblegen.com/nimbledesign/app). The final set of DNA probes was

137   expected to cover 99.7% of the targeted regions. In addition to the previously

138   published *TBX6* gene featuring a compound heterozygous inheritance model (Wu *et*

139   *al.* 2015), the *FBN1* gene was also targeted in the panel. A targeted sequence

140   enrichment library was prepared following a previously described protocol (ASAN *et*

141   *al.* 2011). For each sample, 1 μg of genomic DNA was used as starting material.

142   Genomic DNA was fragmented to a size of ~200-250 bp. The fragmented DNA was

143   end-repaired, capped with A-tailing and subject to ligation of indexed adaptors. After

144   5 cycles of PCR amplification, each indexed product was pooled and hybridized with

145   DNA probes for targeted capture in one solution capture reaction. The product of

146   targeted enrichment DNA was further subject to 14 cycles of PCR amplification,

147   followed by final library yield validation by Bioanalyzer analysis (Agilent, USA) and

148   qPCR quantification. Sequencing was performed with the PE100 mode on an Illumina

149   Hiseq2500 sequencer (Illumina, CA, USA).

150   After generating raw sequence data, a perl script was used to remove low-quality

151   and adaptor-contaminated reads. The remaining reads were mapped onto human

152   reference genome assembly hg19 (GRCh37, http://genome.ucsc.edu/) with the BWA

153   mapper. Additionally, single nucleotide variants (SNVs) and small insertions and

154   deletions (indels) were called with the GATK (v2.2-3) bioinformatics package.

155   Variants were annotated using an in-house developed annotation pipeline. We filtered

156   out variants with common and high frequencies (Minor allele frequency >1%) in the

157   public databases (the 1000 Genomes Project, the Exome Sequencing Project 6500

158   (http://evs.gs.washington.edu/EVS/), ExAC (http://exac.broadinstitute.org) or an

159   in-house WES control dataset) that were also not functionally relevant (deep intronic

160   (>30bp), untranslated regions, or synonymous SNVs, or noncoding indels). We also

161   annotated the detected variants using a customized database based on the Human

162   Gene Mutation Database (HGMD) and Online Mendelian Inheritance in Man (OMIM)

163   (https://omim.org/).

Sanger sequencing

165   Genomic DNA from all individuals was subjected to Sanger sequencing for

166   orthogonal confirmation of all identified variants.

Prediction of probability of NMD events

168   For allelic truncating frameshift variants identified in our cohort and previously

169   reported, *in-silico* predictions of NMD events were implemented using the online

170   NMDEscPredictor (COBAN-AKDEMIR *et al.* 2018).

Plasmid construction and mutagenesis

172   A cDNA fragment containing full-length *FBN1* (GenBank ID: NM_000138.4)

173   cDNA derived from human muscle and having suitable restriction sites was

174   PCR-amplified using KOD-Plus-Neo (Toyobo, Japan). The PCR amplicons were

175   cloned into the *Nhe*I and *Sac*II sites of the pEGFP-N1 expression vector (Clontech,

176   Takara Bio, Japan). Mutant EGFP-FBN1 plasmids were generated by site-directed

177   mutagenesis and their construction confirmed by direct Sanger dideoxy sequencing.

178   G2003R which was previously reported in an adolescent idiopathic scoliosis (AIS)

179   case was used as a positive control (BUCHAN *et al.* 2014). Mutations of

180   Tyr2596Thrfs*86, Glu2759Cysfs*9 and G2003R were introduced into a wild-type

181   (WT) pEGFP-FBN1 QuikChange Lightning Site-directed Mutagenesis Kit (Agilent

182   Technologies, CA, USA) according to the manufacturer's instructions. The resulting

183   three mutant plasmids pEGFP-FBN1-Tyr2596Thrfs*86,

184   pEGFP-FBN1-Glu2759Cysfs*9 and pEGFP-FBN1-Gly2003Arg were used for

185   functional studies.

186   **Cell culture and transfection**

187   HEK293T cells were cultured in DMEM (Gibco, Waltham, MA, USA) + 10%

188   FCS (Biological Industries, Cromwell, USA) + 1% penicillin/streptomycin

189   (Gibco-Life Technologies, USA) at 37°C with 5% CO_2. Cells were

190   transfected/co-transfected with a mutant and/or a WT pEGFP-FBN1 using

191   Lipofectamine3000 (Invitrogen, CA, USA) according to the manufacturers'

192   instructions. Six hours after transfection, the medium was replaced with fresh

193   complete DMEM culture medium, and the cells were further incubated for 48 h. Total

194   proteins were extracted and analyzed by Western blot and SDD-AGE, respectively.

195   **Western blot**

196   Cells were lysed with modified RIPA (50 mM Tris-HCL, 1% NP40, 0.25%

197   Na-deoxycholate, 150 mM NaCl, and 1 mM EDTA; Complete[TM] Protease Inhibitor

198   Cocktail [Roche]), and protein concentrations were determined with the BCA-Kit

199   (Pierce). A total amount of 5 mg protein was size separated on an 8% SDS

200   polyacrylamide gel, and proteins were electrophoresed and transferred to

201   nitrocellulose membranes. Membranes were blocked in powdered milk for 30 min at

202   room temperature (RT, 25-degrees Celsius), and primary antibodies (Phospho-Smad2

203   (Ser245/250/255) Antibody, Cell Signaling Technology; anti-GAPDH, Millipore)

204   were incubated overnight at 4°C. After washing, the corresponding

205   horseradish-peroxidase-coupled goat anti-rabbit secondary antibodies (KPL) were

206   incubated for 1h at RT. Bands were visualized with the WesternBright ECL

207   chemiluminescence system (Advansta, CA, USA). This experiment was performed

208   three times with different cell lysates. Chemiluminescent signals were quantified

209   using ImageJ (SCHNEIDER *et al.* 2012).

210   **SDD-AGE**

211   For Semi-Denaturing Detergent-Agarose Gel Electrophoresis (SDD-AGE)

212   (BERCHOWITZ *et al.* 2015), HEK293T cells were co-transfected with wildtype

213   (pEGFP-FBN1) and mutants (pEGFP-FBN1-Tyr2596Thrfs*86;

214   pEGFP-FBN1-Glu2759Cysfs*9) for 6 h, and then incubated for 48 h. After 48 h

215   incubation at 37°C with 5% CO_2 in the thermotank, cells were harvested by

216   centrifugation at 3000 rcf for 2 min, resuspension in 200 µL water, and subsequent

217   centrifugation. Approximately 100 µl of acid-washed cells were then added to each

218   well followed by 120 µL lysis buffer (100 mM Tris pH 8, 1% Triton X-100, 50 mM

219   β-mercaptoethanol, 3% HALT protease inhibitor cocktail, 30 mM N-ethylmaleimide,

220   and 12.5 U/mL Benzonase nuclease). Blocks were then sealed with a rubber mat

221   (Nunc 276002) and shaken at max speed two times for 3 min on a Qiagen Tissuelyzer

222   2. To each well was then added 35 µL 4X sample buffer (2X TAE, 20% glycerol, 8%

223   SDS, 0.01% bromophenol blue). The blocks were then vortexed briefly and allowed to

224   incubate at RT for three minutes, followed by centrifugation for 2 min at 3000 rcf to

225   remove cell debris. Electrophoresis and capillary blotting to Hybond ECL

226   nitrocellulose were performed as described. Proteins were transferred to a

227   polyvinylidene difluoride membrane and probed with well-characterized monoclonal

228   antibody of anti-Fibrillin 1 (Abcam ab124334, Cambridge, UK).

229   **Statistical analysis**

230   SPSS software, version 17.0 (IBM Corporation; USA), was used to conduct

231   student's two-tailed t-test comparing values of test and control samples. *P*-values of

232   less than 0.05 were considered statistically significant.

233   **Data availability statement**

234   All reagents and plasmids are available upon request. Table S1 and S2 contain a

235   list and descriptions of summary statistics of targeted genes for CS panel and targeted

236   sequencing of 564 genes, respectively. Supplemental files have been submitted to

237   figshare. All mutations identified in this study have been submitted to the Clinvar

238   database (Accession ID: VCV000617941, VCV000617942, VCV000617943).

239

240   **Results**

241   **Clinical characterization and novel allelic variants of individuals with**

242   **MFS/Marfanoid disease**

243   **Subject XH253**. The proband was a 10-year-old Chinese girl (**Fig.1A-D**) who

244   presented with kyphoscoliosis confirmed by radiologic imaging. She was referred to

245   our orthopedic spine specialist for further evaluation and management. Whole-spine

246   X ray examination revealed scoliosis with three curves. Cobb angle of the major

247   curvature was 43 degrees, and she displayed a flat back and thoracolumbar kyphosis.

248   Transthoracic echocardiographic evaluation revealed moderate mitral valve

249   insufficiency and an aortic root measurement of 3.6 cm (Z-score=4.5 when

250   standardized to age and body surface area). Skeletal system abnormalities such as long

251   and thin limbs, and arachnodactyly were observed in the proband.

252   Diminution of vision (myopia) occurred when she was 5 years old. The proband

253   fulfilled the clinical criteria for classical MFS according to Ghent classification

254   (**Table.1**), with a total of 7 points for the score in the revised Ghent Criteria (LOEYS *et*

255   *al.* 2010).A heterozygous frameshift deletion c.7785delC (p.Tyr2596Thrfs*86) was

256   identified in *FBN1* (RefSeq transcript number: NM_000138.4) in the proband via

257   targeted NGS, and subsequently confirmed by further validation using an orthogonal

258   experimental approach of Sanger sequencing (**Fig.1E**).

259   **Subject XH474**. The proband was a 16-year-old Chinese girl (**Fig.1F, G**) who

260   presented with *pectus excavatum* and scoliosis confirmed by radiologic imaging.

261   Transthoracic echocardiographic evaluation revealed anterior mitral leaflet prolapse

262   and moderate mitral valve insufficiency and an aortic root diameter measurement at

263   the level of the sinuses of Valsalva of 2.6 cm (Z-score=1.3 when standardized to age

264   and body surface area). Skeletal system abnormalities were present, such as tall stature

265   with a height of 171 cm (P_{97}; +3SD), slender body habitus with a weight of 48 kg (P_{25},

266   -1SD), and very thin and long upper and lower limbs. Both of her hands indicated an

267   appearance of arachnodactyly; wrist sign and thumb sign were positive. According to

268   the revised Ghent nosology in 2010, an *FBN1* mutation is identified in this sporadic

269   case but aortic root measurements are still below Z score=3 (Z=1.3), the term

270   'potential MFS' should be proposed to use until the aorta reaches threshold. Herein,

271   the second patient here should be categorized as 'potential MFS' (**Table.1**), with a

272   total of 8 points for the systemic score according to the revised Ghent Criteria (LOEYS

273   *et al.* 2010). Heterozygous *FBN1* missense variants c.4890_4891delGTinsTG

274   (p.Gln1630_Cys1631delinsHisGly) were identified in the proband via targeted NGS

275   and validated by Sanger sequencing (**Fig.1H**). The missense variants were confirmed

276   to be *in cis* and comprising a complex allele resulting from a dinucleotide variant by

277   visualizing read alignment views from the Integrative Genomics Viewer (IGV)

278   (**Fig.1I**). Notably, the missense variant of c.4891T>G (p.Cys1631Gly) has been

279   previously reported as a disease-causing mutation in a classical MFS individual,

280   whose clinical course and phenotype was characterized by aortic root dissection,

281   aortic root dilation, mitral valve regurgitation, tricuspid valve prolapse, *ectopia lentis*

282   (ARBUSTINI *et al.* 2005). Conservation analysis of amino acid residues of Gln1630

283   and Cys1631in *FBN1* demonstrate that they are highly conserved throughout

284   evolution and across many selected species, suggesting they are required for the

285   normal function of the protein. Thus, the monoallelic missense variants were most

286   likely damaging and putatively deleterious and possibly accounted for 'potential MFS'

287   in this proband (**Fig.1J**).

288   **Subject XH601**. The proband was a 9-year-old Chinese girl (**Fig.1K, L**). When

289   she was 4 years old at the time of her first evaluation, she presented with a height of

290   101 cm (P_{25}; -1SD), an extremely thin body habitus with a weight of 12 kg (P_3, -3SD).

291   Physical examination revealed bilateral arachnodactyly (**Fig.1M, N**), uneven

292   asymmetric back whilst bending and congenital dislocation of the hip joint.

293   Whole-spine X ray examination displayed severe right thoracic scoliosis with a main

294   Cobb angle of 117 degrees (**Fig.1O, P**). Transthoracic echocardiogram demonstrated

295   anterior and posterior mitral leaflet prolapse and moderate mitral valve insufficiency

296   without apparent aortic diameter enlargement at the sinuses of Valsalva or aortic root

297   dissection. Ocular system abnormalities indicated bilateral down-slanting palpebral

298   fissures, epicanthus and astigmatism. However, there were no signs or symptoms of

299   ectopia lentis. The predominant features in this patient were an extreme congenital

300   lack of subcutaneous fat, consistent with a lipodystrophy by physical exam, and a

301 subsequent bodily progeroid appearance. However, this proband did not meet revised

302 Ghent Criteria for classical MFS. Consecutive follow-ups and assessment of the

303 proband were conducted. Upon genotype driven reverse phenotyping of the proband

304 when she was 9, the proportion of upper and lower segment lengths was basically

305 normal with a ratio of 0.87. The proband had a height of 136 cm (P_{50} ,0). For

306 comparison, her father's height measurement was 170 cm and her mother's was 160

307 cm. The body mass index (BMI) of the proband was extremely low (11.1 kg/m^2)

308 potentially due to disproportionate weight gain by age. More specifically, the patient

309 had an extremely thin habitus with a weight of 20.5 Kg (P_3, -3SD). Furthermore, hand

310 and foot radiographs to potentially assess 'bone age' suggested bilateral

311 metacarpophalangeal joint dislocation, interosseous atrophy and dolichostenomelia

312 (**Fig.1Q, R**). The proband was eventually diagnosed with

313 Marfanoid-progeroid-lipodystrophy syndrome (**Table.2**). Through targeted NGS, a

314 heterozygous variant of c.8275_8291delGAGAAGACAGCCATCTT

315 (c.8275_8291del; p.Glu2759Cysfs*9) in *FBN1* was identified in the proband. We

316 consequently confirmed this variant in subject XH601 and it was indeed *de novo*

317 through parental Sanger sequencing and trio analysis (**Fig.1S**). In addition to Sanger

318   sequencing validation, we also performed cloning sequencing on Subject XH601 to

319   further verify that this indel is subject to frame-shift variation (data not shown).

320   Moreover, these two allelic truncating variants of p.Tyr2596Thrfs*86 and

321   p.Glu2759Cysfs*9 were not present in ExAC, 1000 Genome, ESP6500 database,

322   universal mutation database (UMD) (COLLOD-BEROUD *et al.* 2003) and our in-house

323   database (with 2000+ Chinese exomes). Clinical and genetic characteristics of subject

324   XH253 with classical MFS and XH474 with 'potential MFS' based on the revised

325   Ghent Criteria (LOEYS *et al.* 2010) are presented in Table 1.

326

327   **NMD-degradation prediction**

328   The variant of Y2596Tfs*86 identified in XH253 was a single nucleotide

329   frameshift deletion leading to a premature termination codon (PTC) in Exon 64, while

330   E2759Cfs*9 identified in XH601 was a frameshift deletion leading to a PTC in Exon

331   66, the final exon of *FBN1* (**Fig. 2A**). Although both variants are very close in linear

332   space, they may lead to distinct alterations to the *FBN1* transcript. To investigate this

333   hypothesis, we performed NMD predictions of the two truncating variants on

334   NMDescPredictor (COBAN-AKDEMIR *et al.* 2018). The result showed that

335   Y2596Tfs*86 is predicted to be degraded by NMD, i.e. NMD$^+$, while E2759Cfs*9 is

336   predicted to escape NMD, i.e. NMD⁻ (**Fig. 2B**). Using the same analytical tools, we

337   further tested whether previously reported protein-truncating *FBN1* frameshift

338   variants implicated in MPLS subjects (GRAUL-NEUMANN *et al.* 2010; GOLDBLATT *et*

339   *al.* 2011; TAKENOUCHI *et al.* 2013; GARG AND XING 2014) uniformly shared the

340   mechanism of escaping NMD. Our analysis shows that all of the truncating *FBN1*

341   frameshift variants within the C-terminal gene region may escape NMD, supporting

342   the contention that the underlying disease mechanism in MPLS is the same and

343   distinct from MFS (**Fig. 2B**). These findings implicate a mechanism distinct from

344   loss-of-function (LoF) alleles, and potentially gain-of-function (GoF) variant alleles

345   (COBAN-AKDEMIR *et al.* 2018), at the *FBN1* locus causing MPLS.

346

347   **Perturbation of native aggregation process by MPLS-causative truncating**
348   **mutation**

349   To further determine if the mutant FBN1 protein in MPLS is able to lead to

350   dominant   negative   or   GoF   effects,   plasmids   expressing   mutants

351   (pEGFP-FBN1-Tyr2596Thrfs*86; pEGFP-FBN1-Glu2759Cysfs*9) and WT plasmid

352   (pEGFP-FBN1) were co-transfected into HEK293T cells at a 1:1 ratio. After 48h of

353   expression, lysates from cells expressing EGFP-FBN1 fusions were analyzed by

354   SDD-AGE. Detection of SDS-resistant aggregates by SDD-AGE in cell lysates of

355   HEK293T transiently expressing EGFP-FBN1 fusions were investigated with

356   SDD-AGE and Western blot. Protein expression was induced for 48 h and detected

357   with a monoclonal FBN1-specific antibody. Remarkably, WT plasmid (EGFP-FBN1

358   fusions) had the SDS-resistance properties of an amyloidogenic protein structure.

359   Since amyloid formation is time- and concentration-dependent, we set the time of

360   transient expression to 48 h. WT plasmid (EGFP-FBN1 fusions) were aggregated after

361   48 h expression, whereas co-transfection of pEGFP-FBN1-Glu2759Cysfs*9 and WT

362   plasmid resulted in the presence of a small fraction of monomer protein. This suggests

363   that pEGFP-FBN1-Glu2759Cysfs*9 apparently prohibited the native aggregation

364   process of WT plasmid, possibly revealing an intracellular dominant-negative

365   mechanism.   In   addition,   we   observed   that   co-transfection   of

366   pEGFP-FBN1-Tyr2596Thrfs*86 and WT plasmid presented a small fraction of

367   aggregated protein. As this fraction was less than that of the WT plasmid, it can be

368   suggested that Tyr2596Thrfs*86 may undergo an NMD mechanism thus leading to

369   *FBN1* haploinsufficiency (**Fig.3A**). Moreover, these variations in the range of particle

370   sizes were observed, and again were reproducible for individual EGFP-FBN1 fusions

371   validated by another two independent replication experiments.

372

Disruption of downstream TGF-β signaling

Previous studies have demonstrated that deleterious *FBN1* mutations causing Marfan syndrome result in upregulated endogenous transforming growth factor β (TGF-β) receptor signaling (ANDELFINGER *et al.* 2016). Such signaling can be measured in plasma or indirectly measured through aberrant activation of downstream targets, including excessive phosphorylation of SMAD2 (pSMAD2) (VERSTRAETEN *et al.* 2016). To determine the functional consequences of the novel truncating *FBN1* variant of E2759Cfs*9 in the MLPS patient, plasmids expressing mutant EGFP-FBN1 cDNAs were transfected into HEK293T cells. Transfected cells with truncating *FBN1* variants of Y2596Tfs*86 (P=0.007), E2759Cfs*9 (P=0.017) and Gly2003Arg (P=0.006) showed significantly elevated phosphorylation of SMAD2 (pSMAD2) in Western blots compared to the WT plasmid (**Fig.3B, C**). This observation is consistent with the contention that the TGF-β signaling pathway is perturbed in a SMAD-dependent manner in all 3 subjects.

Genotypic and phenotypic features of reported MPLS patients

Intriguingly, the mechanism underlying *FBN1*-related diseases involves either loss-of-function (LoF) or NMD surveillance pathway escape as conveyed by allelic truncating mutations. Such distinct mechanisms could contribute to distinct disease

392   phenotypes of varying severity. According to a previous report, *FBN1* LOF mutations

393   led to classical MFS (PARK *et al.* 2017), while predicted NMD surveillance pathway

394   escape in *FBN1* can cause a MPLS phenotype (ROMERE *et al.* 2016), Patient XH601

395   in our cohort harbored a heterozygous *de novo* variant of E2759Cfs*9 in *FBN1,* which

396   is located in the final exon. Notably, our MPLS patients presented with

397   bilateral down-slanting palpebral fissures, epicanthus and eye astigmatism. The main

398   clinical features of this complicated disorder, clustered in Table 2, include accelerated

399   aging and postnatal lipodystrophy, poor weight gain since birth, premature birth,

400   hyperextensible digits and generalized subcutaneous fat reduction leading to a

401   progeroid appearance of the body in all patients. Mental and motor development

402   remain mostly normal. Overlapping clinical features of MPLS with MFS are

403   phenotypically diverse. Ocular system involvement like myopia have been observed

404   in all individuals, although hyperextensible joints, arachnodactyly, and other

405   significant signs of classical MFS are not always present, i.e. mitral valve prolapse in

406   4/8, lumbosacral dural ectasia in 2/3 (5 data points unavailable), *pectus excavatum* in

407   3/8, and ectopia lentis in 3/8. Scoliosis was reported in two patients aged 23 and 17

408   years, and kyphosis was reported in a patient aged 27 years, but not described in the

409   others (**Table.2**). Remarkably, the major Cobb angles of Subject XH253 with classical

410 MFS and Subject XH474 with MASS were 43 degrees and 85 degrees, respectively.

411 Our MPLS patient presented a thoracic scoliosis with a major Cobb angle magnitude

412 of 117 degrees—a condition much more severe compared to the MFS patients,

413 counterparts.

Discussion

415 In the present report, we provide direct evidence for potential dominant negative

416 alleles in MPLS patients caused by truncating *FBN1* variants escaping NMD. These

417 genetic and functional investigations also include description of the first patient with

418 MPLS of Chinese ancestry.

419 Several case reports previously identified an association between monogenic

420 *FBN1* mutations and reduction of subcutaneous fat and/or progeroid features

421 (GRAUL-NEUMANN *et al.* 2010; GOLDBLATT *et al.* 2011; TAKENOUCHI *et al.* 2013;

422 JACQUINET *et al.* 2014; PASSARGE *et al.* 2016). Here, we have provided further

423 evidence for the existence of a distinct genetic disease, MPLS, caused by *FBN1*

424 mutations. The MPLS patient in our study is characterized by accelerated aging and

425 postnatal lipodystrophy, disproportionate weight gain since birth, severe scoliosis,

426 downslanting palpebral fissures, bilateral metacarpophalangeal joint dislocation,

427   mitral valve prolapse, bilateral interosseous atrophy, and congenital dislocation of the

428   hip. Intriguingly, this patient was previously diagnosed with Marfanoid disease

429   (**Table.1**) due to an unclear molecular diagnosis. We consequently performed targeted

430   NGS on the affected proband and her unaffected parents. As a result, we identified

431   c.8275_8291del(p.Glu2759Cysfs*9) in *FBN1* as the responsible variant for the

432   proband. Sanger sequencing was then conducted on genomic DNA from both parents

433   to confirm the *de novo* occurrence and segregation with phenotypes. Subsequently, we

434   proceeded with a comprehensive phenotypic analysis of all family members through

435   intensive clinical follow-up. By combining genetic data with reverse phenotyping, we

436   eventually diagnosed the proband with MPLS. Notably, the severity of spinal

437   deformity in the MPLS individual was significantly more severe than that in Subject

438   XH253 and XH474 (with classical MFS and potential MFS, respectively). We

439   consider that MPLS is a distinct fibrillinopathy because it can be clinically

440   distinguished from other fibrillinopathies, including classical MFS. To our knowledge,

441   there are no other syndromes that simultaneously comprise the clinical phenotypes of

442   marfanoid features, accelerated aging, postnatal lipodystrophy, poor weight gain since

443   birth, and progeroid appearance. Particularly, the involvement of both reduced

444   subcutaneous fat tissue and progeroid appearance is a prominent characteristic of

445 MPLS. These comprehensive findings predominate in determining the severity of

446 defects in individuals and thus significantly influence the prognosis: lipodystrophic

447 disorders are frequently associated with metabolic disturbance, such as insulin

448 resistance and life-threatening hypertriglyceridemia (VANTYGHEM *et al.* 2012). Such

449 potential metabolic disturbances are particularly important to note prior to surgical

450 intervention as has been noted for the ocular-scoliotic form of Ehlers Danlos

451 syndrome due to lysl hydroyase deficiency (YEOWELL *et al.* 1995). Secondly,

452 elucidation of the phenotype of MPLS has been limited due to the paucity of prior

453 clinical reports, with only seven relevant patients previously described. Up to now, it

454 is known only to be caused by a single gene with a monogenic AD inheritance pattern

455 for the disease trait. Finally, we have shown that, in terms of pathogenic mechanisms,

456 the truncating *FBN1* mutations that cause MPLS cluster in 3' gene regions encoding

457 the extreme C-terminal domains and these variant alleles represent a subset that differ

458 from those that cause classical MFS. Most of such mutations will be anticipated to

459 escape NMD and we propose these to function via a potential mechanism between

460 GoF and dominant negative and not a LoF mechanism.

461 Fibrillin-1 acts as the precursor to a recently-described glucogenic hormone:

462 aprosin (DAVIS *et al.* 2016a). Specifically, Exon 65 of *FBN1* encodes 11 amino acids,

463   while Exon 66 of *FBN1* encodes 129 amino acids of asprosin (ROMERE *et al.* 2016).

464   Recently, Chen et.al. have successfully constructed a gene-edited rabbit model with a

465   truncated C-terminus of fibrillin-1 involving the ultimate two exons which could

466   recapitulate the histopathological alterations and functional defects associated with

467   MPLS (CHEN *et al.* 2018). Since individuals with low fibrillin-1 level may fail to

468   differentiate adipocytes and/or to accumulate adipocyte lipids, truncating variants

469   located adjacent to the two exons of *FBN1* are prone to cause lipodystrophic

470   phenotypes (DAVIS *et al.* 2016b).

471   PTCs located in the final coding exon are specifically prone to escape NMD and so

472   are processed distinctly from those in internal exons in terms of transcript degradation,

473   leading to the stable translation of truncated proteins (BAYRAM *et al.* 2017). Excessive

474   amounts of mutated protein are therefore produced (INOUE *et al.* 2004), leading to a

475   dominant negative molecular mechanism and the severe MPLS disease phenotype.

476   Consistent with this interpretation, all truncating mutations associated with MPLS are

477   located adjacent to the penultimate exon (Exon 65) and are predicted to escape NMD

478   (**Figure.4**). From this perspective, it is perhaps most parsimonious to postulate that the

479   incorporation of relatively few mutant monomers would be sufficient to impair the

480   systemic processes of microfibrillar assembly and function.

481   Aberrant activation of the TGF-β pathway has been observed in MFS and may

482   account for some of the musculoskeletal deformities, such as scoliosis (BUCHAN *et al.*

483   2014). The MPLS patient with a truncating *FBN1* variant presented with severe

484   scoliosis, which suggests that the protein change also alters TGF-β signaling. Our

485   results showed upregulation of the TGF-β pathway in plasmids expressing mutant

486   EGFP-FBN1 cDNAs, confirming that the variant of E2759Cfs*9 identified in the

487   MPLS patient has functional effects in a SMAD-dependent manner in all 3 subjects.

488   Our study indicated that the two phenotypes associated with *FBN1* mutations,

489   MPLS and MFS are caused by two distinct molecular mechanisms. The more severe

490   phenotype of MPLS, which had its first report in the Chinese population, is caused by

491   nonsense mutations that produce truncated *FBN1* mutant proteins. These proteins

492   disrupt the process of native amyloid-like structure conformation and exert potent

493   intracellular dominant-negative activity. In this view, abnormal protein derived from

494   the mutant allele interacts and interferes with protein derived from the normal allele,

495   consequently resulting in substantial loss of function. Supportive evidence includes (a)

496   *de novo* monogenic AD inheritance pattern, and (b) aggregation of fibrillin-1 in which

497   the mutated monomer derived from the mutant allele impairs the fundamental

498   structure of its wildtype protein derived from the normal allele counterpart. This

499 deficiency could be supported by SDD-AGE analysis, suggesting that dominant

500 negative interference is not restricted to enhanced proteolytic clearance of mutant

501 microfibrils over time (BRENN *et al.* 1996), but rather could also occur at the level of

502 intracellular aggregate formation processes. The more moderate phenotype, classical

503 MFS, is caused by nonsense mutations that activate the NMD RNA surveillance

504 pathway, thereby degrading mutant transcripts and resulting in *FBN1*

505 haploinsufficiency. The data support the concept of distinct pathogenetic mechanisms,

506 GoF *versus* LoF (BAYRAM *et al.* 2017; COBAN-AKDEMIR *et al.* 2018; POLI *et al.* 2018),

507 for each well-established subgroup of fibrillinopathy, which mostly hinges on the

508 intrinsic features of fibrillin-1 mutations. It is of crucial significance to pinpoint and

509 appreciate the locus heterogeneity, clinical relevance and overlapping clinical features

510 with other syndromes/disorders in a phenotype-oriented approach that characterizes

511 much of clinical medicine practice (WHITE *et al.* 2018).

512 In conclusion, we provide direct evidence of dominant negative effects of

513 truncating *FBN1* variants predicted to escape NMD in MPLS patients. Our study

514 expands the mutational spectrum of *FBN1* and highlights the potential molecular

515 mechanism for MPLS patients, which facilitates our understanding of

516 genotype-phenotype correlations in terms of *FBN1* to provide effective genetic

517 counseling, implementation and timing of therapy (e.g. mitigation of TGF-β

518 hypersignaling, surgical intervention for cardiovascular complications or for

519 scoliosis), or early intervention.

Acknowledgments

535   K08 HG008986 to J.E.P.).

536

Conflict of interest

545

References

547   Andelfinger, G., B. Loeys and H. Dietz, 2016 A Decade of Discovery in the Genetic

548   Understanding of Thoracic Aortic Disease. Can J Cardiol 32: 13-25.

549   Arbustini, E., M. Grasso, S. Ansaldi, C. Malattia, A. Pilotto et al., 2005 Identification

550   of sixty-two novel and twelve known *FBN1* mutations in eighty-one

551   unrelated probands with Marfan syndrome and other fibrillinopathies. Hum

552   Mutat 26: 494.

Asan, Y. Xu, H. Jiang, C. Tyler-Smith, Y. Xue et al., 2011 Comprehensive comparison of three commercial human whole-exome capture platforms. Genome Biol 12: R95.

Bayram, Y., J. J. White, N. Elcioglu, M. T. Cho, N. Zadeh et al., 2017 REST Final-Exon-Truncating Mutations Cause Hereditary Gingival Fibromatosis. Am J Hum Genet 101: 149-156.

Berchowitz, L. E., G. Kabachinski, M. R. Walker, T. M. Carlile, W. V. Gilbert et al., 2015 Regulated Formation of an Amyloid-like Translational Repressor Governs Gametogenesis. Cell 163: 406-418.

Brenn, T., T. Aoyama, U. Francke and H. Furthmayr, 1996 Dermal fibroblast culture as a model system for studies of fibrillin assembly and pathogenetic mechanisms: defects in distinct groups of individuals with Marfan's syndrome. Lab Invest 75: 389-402.

Buchan, J. G., D. M. Alvarado, G. E. Haller, C. Cruchaga, M. B. Harms et al., 2014 Rare variants in *FBN1* and *FBN2* are associated with severe adolescent idiopathic scoliosis. Hum Mol Genet 23: 5271-5282.

Chen, M., B. Yao, Q. Yang, J. Deng, Y. Song et al., 2018 Truncated C-terminus of fibrillin-1 induces Marfanoid-progeroid-lipodystrophy (MPL) syndrome in

571   rabbit. Dis Model Mech 11.

572   Coban-Akdemir, Z., J. J. White, X. Song, S. N. Jhangiani, J. M. Fatih et al., 2018

573   Identifying Genes Whose Mutant Transcripts Cause Dominant Disease Traits

574   by Potential Gain-of-Function Alleles. Am J Hum Genet 103: 171-187.

575   Collod-Beroud, G., S. Le Bourdelles, L. Ades, L. Ala-Kokko, P. Booms et al., 2003

576   Update of the UMD-FBN1 mutation database and creation of an *FBN1*

577   polymorphism database. Hum Mutat 22: 199-208.

578   Davis, M. R., E. Arner, C. R. Duffy, P. A. De Sousa, I. Dahlman et al., 2016a

579   Datasets of genes coexpressed with *FBN1* in mouse adipose tissue and during

580   human adipogenesis. Data Brief 8: 851-857.

581   Davis, M. R., E. Arner, C. R. Duffy, P. A. De Sousa, I. Dahlman et al., 2016b

582   Expression of *FBN1* during adipogenesis: Relevance to the lipodystrophy

583   phenotype in Marfan syndrome and related conditions. Mol Genet Metab 119:

584   174-185.

585   Dietz, H. C., 2015 Potential Phenotype-Genotype Correlation in Marfan Syndrome:

586   When Less is More? Circ Cardiovasc Genet 8: 256-260.

587   Duerrschmid, C., Y. He, C. Wang, C. Li, J. C. Bournat et al., 2017 Asprosin is a

588   centrally acting orexigenic hormone. Nat Med 23: 1444-1453.

589   Garg, A., and C. Xing, 2014 De novo heterozygous *FBN1* mutations in the extreme

590   C-terminal region cause progeroid fibrillinopathy. Am J Med Genet A 164a:

591   1341-1345.

592   Goldblatt, J., J. Hyatt, C. Edwards and I. Walpole, 2011 Further evidence for a

593   marfanoid syndrome with neonatal progeroid features and severe generalized

594   lipodystrophy due to frameshift mutations near the 3' end of the *FBN1* gene.

595   Am J Med Genet A 155a: 717-720.

596   Graul-Neumann, L. M., T. Kienitz, P. N. Robinson, S. Baasanjav, B. Karow et al.,

597   2010 Marfan syndrome with neonatal progeroid syndrome-like lipodystrophy

598   associated with a novel frameshift mutation at the 3' terminus of the

599   FBN1-gene. Am J Med Genet A 152a: 2749-2755.

600   Inoue, K., M. Khajavi, T. Ohyama, S. Hirabayashi, J. Wilson et al., 2004 Molecular

601   mechanism for distinct neurological phenotypes conveyed by allelic

602   truncating mutations. Nat Genet 36: 361-369.

603   Jacquinet, A., A. Verloes, B. Callewaert, C. Coremans, P. Coucke et al., 2014

604   Neonatal progeroid variant of Marfan syndrome with congenital

605   lipodystrophy results from mutations at the 3' end of *FBN1* gene. Eur J Med

606   Genet 57: 230-234.

607   Loeys, B. L., H. C. Dietz, A. C. Braverman, B. L. Callewaert, J. De Backer et al.,

608   2010 The revised Ghent nosology for the Marfan syndrome. J Med Genet 47:

609   476-485.

610   Park, J. W., L. Yan, C. Stoddard, X. Wang, Z. Yue et al., 2017 Recapitulating and

611   Correcting Marfan Syndrome in a Cellular Model. Int J Biol Sci 13: 588-603.

612   Passarge, E., P. N. Robinson and L. M. Graul-Neumann, 2016

613   Marfanoid-progeroid-lipodystrophy syndrome: a newly recognized

614   fibrillinopathy. Eur J Hum Genet 24: 1244-1247.

615   Poli, M. C., F. Ebstein, S. K. Nicholas, M. M. de Guzman, L. R. Forbes et al., 2018

616   Heterozygous Truncating Variants in *POMP* Escape Nonsense-Mediated

617   Decay and Cause a Unique Immune Dysregulatory Syndrome. Am J Hum

618   Genet 102: 1126-1142.

619   Romere, C., C. Duerrschmid, J. Bournat, P. Constable, M. Jain et al., 2016 Asprosin,

620   a Fasting-Induced Glucogenic Protein Hormone. Cell 165: 566-579.

621   Schneider, C. A., W. S. Rasband and K. W. Eliceiri, 2012 NIH Image to ImageJ: 25

622   years of image analysis. Nat Methods 9: 671-675.

623   Song, Y. H., G. H. Kim, H. W. Yoo and J. B. Kim, 2012 Novel de novo nonsense

624   mutation of *FBN1* gene in a patient with Marfan syndrome. J Genet 91:

625   233-235.

626   Takenouchi, T., M. Hida, Y. Sakamoto, C. Torii, R. Kosaki et al., 2013 Severe

627   congenital lipodystrophy and a progeroid appearance: Mutation in the

628   penultimate exon of *FBN1* causing a recognizable phenotype. Am J Med

629   Genet A 161a: 3057-3062.

630   Vantyghem, M. C., A. S. Balavoine, C. Douillard, F. Defrance, L. Dieudonne et al.,

631   2012 How to diagnose a lipodystrophy syndrome. Ann Endocrinol (Paris) 73:

632   170-189.

633   Verstraeten, A., M. Alaerts, L. Van Laer and B. Loeys, 2016 Marfan Syndrome and

634   Related Disorders: 25 Years of Gene Discovery. Hum Mutat 37: 524-531.

635   White, J. J., J. F. Mazzeu, Z. Coban-Akdemir, Y. Bayram, V. Bahrambeigi et al.,

636   2018 WNT Signaling Perturbations Underlie the Genetic Heterogeneity of

637   Robinow Syndrome. Am J Hum Genet 102: 27-43.

638   Wu, N., X. Ming, J. Xiao, Z. Wu, X. Chen et al., 2015 *TBX6* null variants and a

639   common hypomorphic allele in congenital scoliosis. N Engl J Med 372:

640   341-350.

641   Yeowell, H. N., L. C. Walker, M. K. Marshall, S. Murad and S. R. Pinnell, 1995 The

642   mRNA and the activity of lysyl hydroxylase are up-regulated by the

643   administration of ascorbate and hydralazine to human skin fibroblasts from a

644   patient with Ehlers-Danlos syndrome type VI. Arch Biochem Biophys 321:

645   510-516.

646

647 **Figure Legends**

648 **Figure 1** Clinical and genetic manifestations of the research subjects

649 (A, B) Pictures of patient XH253 indicated bilateral arachnodactyly of hands and

650 feet.

651 (C, D) The anterior and lateral view of Patient XH253 demonstrated scoliosis on

652 whole-spine X-ray images.(E) Sanger sequencing of XH253 verified a novel

653 heterozygous frameshift variant of p.Tyr2596Thrfs*86 in *FBN1*. (F, G) The anterior

654 and lateral view of subject XH474 demonstrated scoliosis on whole-spine X-ray

655 images. (H) Sanger sequencing verified monoallelic missense mutations of

656 p.Gln1630His and p.Cys1631Gly in *FBN1*. (I) Integrative Genomics Viewer (IGV)

657 displays varying level of alignment reads detail depending on the zoom level and

658 uses red box and transparency to highlight monoallelic missense variants in the

659 exome data from XH474.

660 (J) Conservation analysis of amino acid residues of *FBN1* among vertebrates.

661 Lines indicate homologous amino acid sequences in selected vertebrates. Note the

662 strong conservation of Cys1631 among vertebrates highlighted in red and Gln1630

663 highlighted in green, respectively. (K, L, M, N) Photographic images of subject

664 XH601 who presented with scoliosis, short stature and subcutaneous fat reduction

665   and arachnodactyly anomalies of hands and feet.(O, P) The anterior and lateral view

666   demonstrated severe scoliosis on whole-spine X-ray images.

667   (Q, R) Hand and foot radiographs showed bilateral metacarpophalangeal dislocation,

668   interosseous atrophy, claw hands and dolichostenomelia. (S) Sanger sequencing of

669   XH601 parent-offspring trio verified a novel de novo heterozygous frameshift

670   mutation of p.Glu2759Cysfs*9 in *FBN1*. The RefSeq transcript number of *FBN1* is

671   NM_000138.4.

672

673   **Figure 2** Schematic representations and NMD predictions of the p.Y2596Tfs*86 and

674   p.E2759Cfs*9 mutations other MPLS-affected frameshift mutations in *FBN1*

675   (A) Schematic diagrams of full-length WT and mutant EGFP-FBN1 plasmids

676   transiently expressed in HEK293T. The numbers indicate the amino acid positions in

677   *FBN1*. PTC location is marked with red circle. The resulting frameshift and

678   reduction in the deduced amino acid sequence caused by the p.Y2596Tfs*86 and

679   p.E2759Cfs*9 mutations are indicated by the yellow region, respectively.

680   (B) Prediction of frameshift variants that are potentially subject to

681   nonsense-mediated mRNA decay (NMD)-escape or NMD-degradation. The

682   mutation of p.Y2596Tfs*86 in *FBN1* gene is predicted to be subject to degradation

683   by triggering NMD. The p.E2759Cfs*9 mutation in *FBN1* gene is predicted to

684   escape NMD. All of other MPLS-affected frameshift mutations in *FBN1* are

685   predicted to escape NMD.

686

687   **Figure 3** Functional effects of the Y2596Tfs*86 and E2759Cfs*9 mutations on

688   *FBN1* protein expression

689   (A) Detection of SDS-resistant aggregates by SDD-AGE in cell lysates of HEK293T

690   transiently expressing EGFP-FBN1 fusions were investigated by SDD-AGE and

691   Western blot. Expression of the proteins was induced for 48 h and detected with a

692   monoclonal FBN1-specific antibody.

693   (B) Elevated phosphorylation of SMAD2 (pSMAD2) in individuals with truncating

694   *FBN1* variants, respectively. G2003R is used as a positive control. GAPDH is used

695   as a loading control. pSMAD2/GAPDH ratio is shown normalized to the unaffected

696   control (WT).

697   (C) Gray-scale analysis results show significantly upregulated (pSMAD2) in

698   constructs encoding truncating *FBN1* variants. EV denotes empty vector (pEGFP).

699   RT: room temperature. Data are represented as mean ± SD of three independent

700   experiments.   * denotes   P value ＜0.05 and ** denotes   P value ＜0.01.

701

702 **Figure 4** The partial gene structure of the C-terminus of *FBN1* and overview of

703 previously reported truncating variants in and around Exon 65 in patients presenting

704 with MPLS

705 Blue, purple and red boxes denote specific domain. Light green, orange and black

706 boxes denote exons and the gray area between the two boxes denote introns. All

707 truncating variants were annotated by small green circles except that c.8226+1G>T

708 previously reported twice was annotated by a big circle. COOH denotes COOH

709 unique region. Deep blue box denotes purported asprosin encoded by the exons of
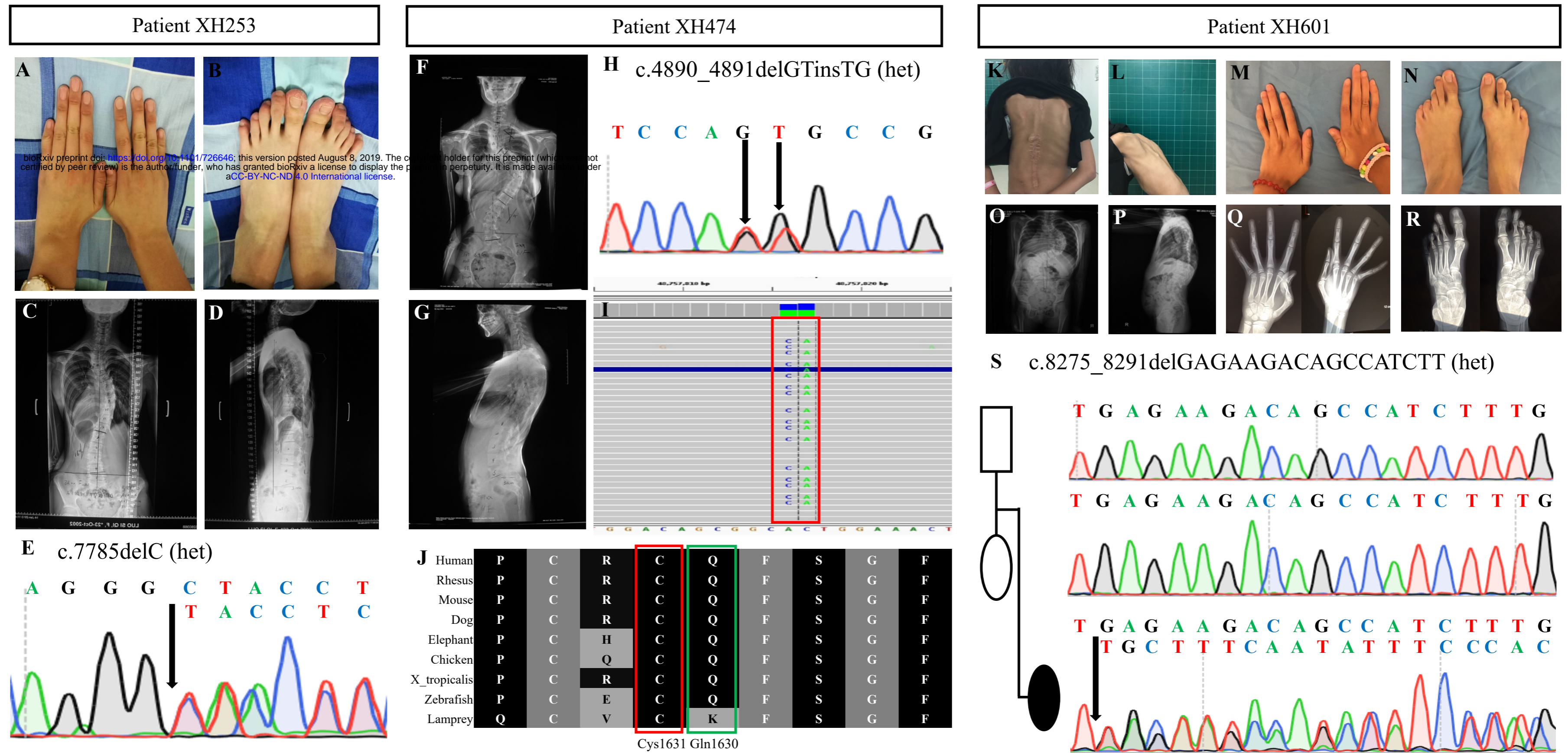
710 *FBN1*.

711

712

713

714

Figure 1

Patient XH253

A   B

C   D

E   c.7785delC (het)

A G G G C T A C C T
        T A C C T C

Patient XH474

F

G

H   c.4890_4891delGTinsTG (het)

T C C A G T G C C G

I   40,757,810 bp   40,757,820 bp

GGACAGCGGGCACTGGAAACT

J

	Human	P	C	R	C	Q	F	S	G	F
	Rhesus	P	C	R	C	Q	F	S	G	F
	Mouse	P	C	R	C	Q	F	S	G	F
	Dog	P	C	R	C	Q	F	S	G	F
	Elephant	P	C	H	C	Q	F	S	G	F
	Chicken	P	C	Q	C	Q	F	S	G	F
	X_tropicalis	P	C	R	C	Q	F	S	G	F
	Zebrafish	P	C	E	C	Q	F	S	G	F
	Lamprey	Q	C	V	C	K	F	S	G	F

Cys1631 Gln1630

Patient XH601

K   L   M   N

O   P   Q   R

S   c.8275_8291delGAGAAGACAGCCATCTT (het)

T G A G A A G A C A G C C A T C T T T G

T G A G A A G A C A G C C A T C T T T G

T G A G A A G A C A G C C A T C T T T G
T G C T T T C A A T A T T T C C A C

Figure 2

A

FBN1-WT

FBN1-Y2596Tfs*86

FBN1-E2759Cfs*9

c.8175_8182delACGGGGCA
(p. Arg2726Glufs*9):
Escaping NMD

c.8206_8207insA
(p.Thr2736Asnfs*1):
Escaping NMD

c.8156_8175delAA
(p.Lys2719Thrfs*12):
Escaping NMD

c.8155_8156delAA
(p.Lys2719Aspfs*18):
Escaping NMD

c.7785delC
(p.Tyr2596Thrfs*86):
Triggering NMD

B

c.8275_8291del
(p.Glu2759Cysfs*9):
Escaping NMD

Information

- Canonical stop
- CDS start
- Your variant location

Color

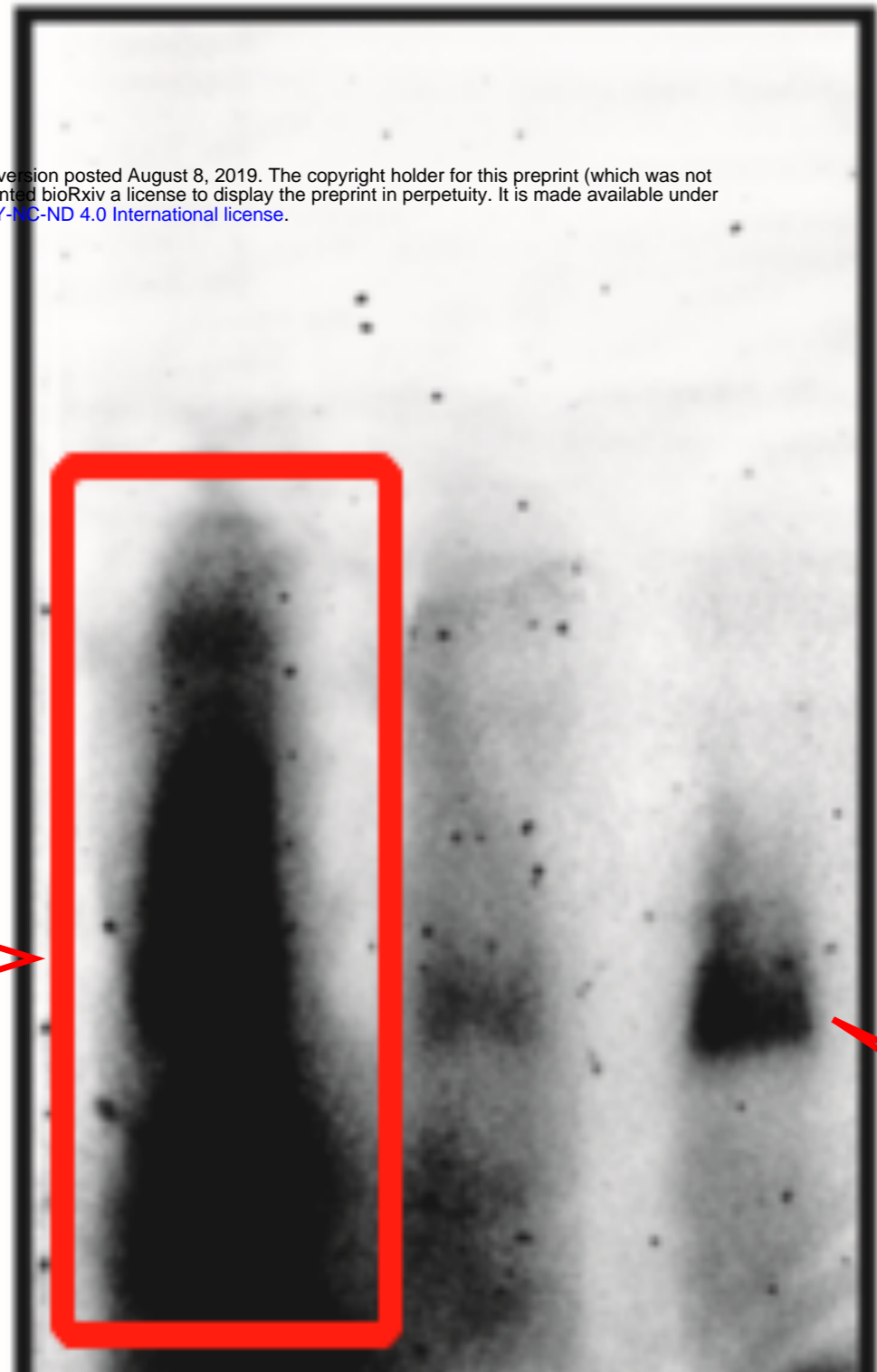- NMD-competent region
- NMD-incompetent region
- Nonstop region

Figure 3

A

Temperature — RT

HEK293T

Anti-FBN1

Aggregate

Monomer

FBN1-WT	+	+	+
FBN1-Y2596Tfs*86	-	+	-
FBN1-E2759Cfs*9	-	-	+

B

WT   p.Y2596Tfs*86   p.E2759Cfs*9   p.G2003R
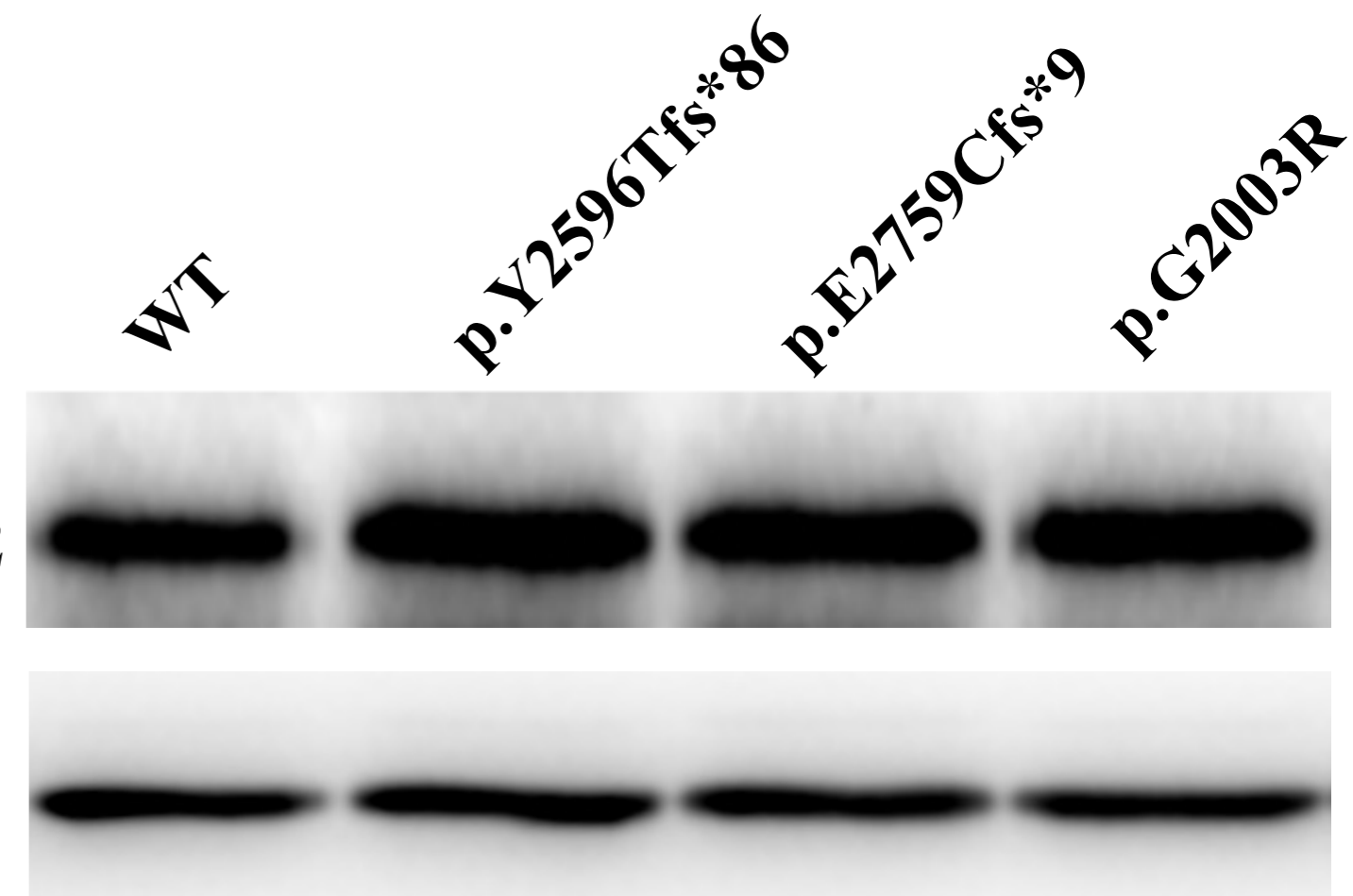
P-SMAD2

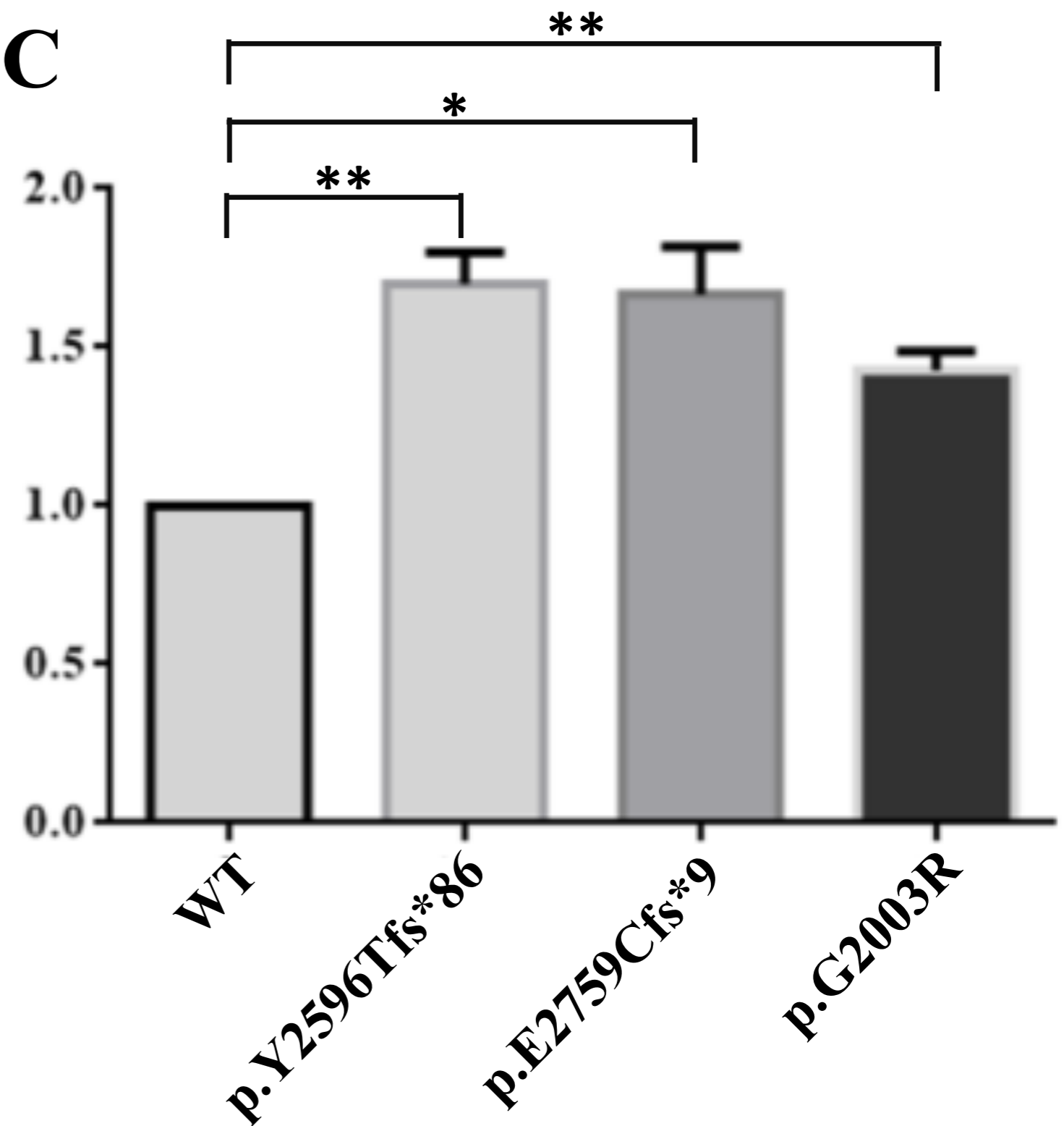GAPDH

P-SMAD2/GAPDH   1.0   1.8   1.8   1.4
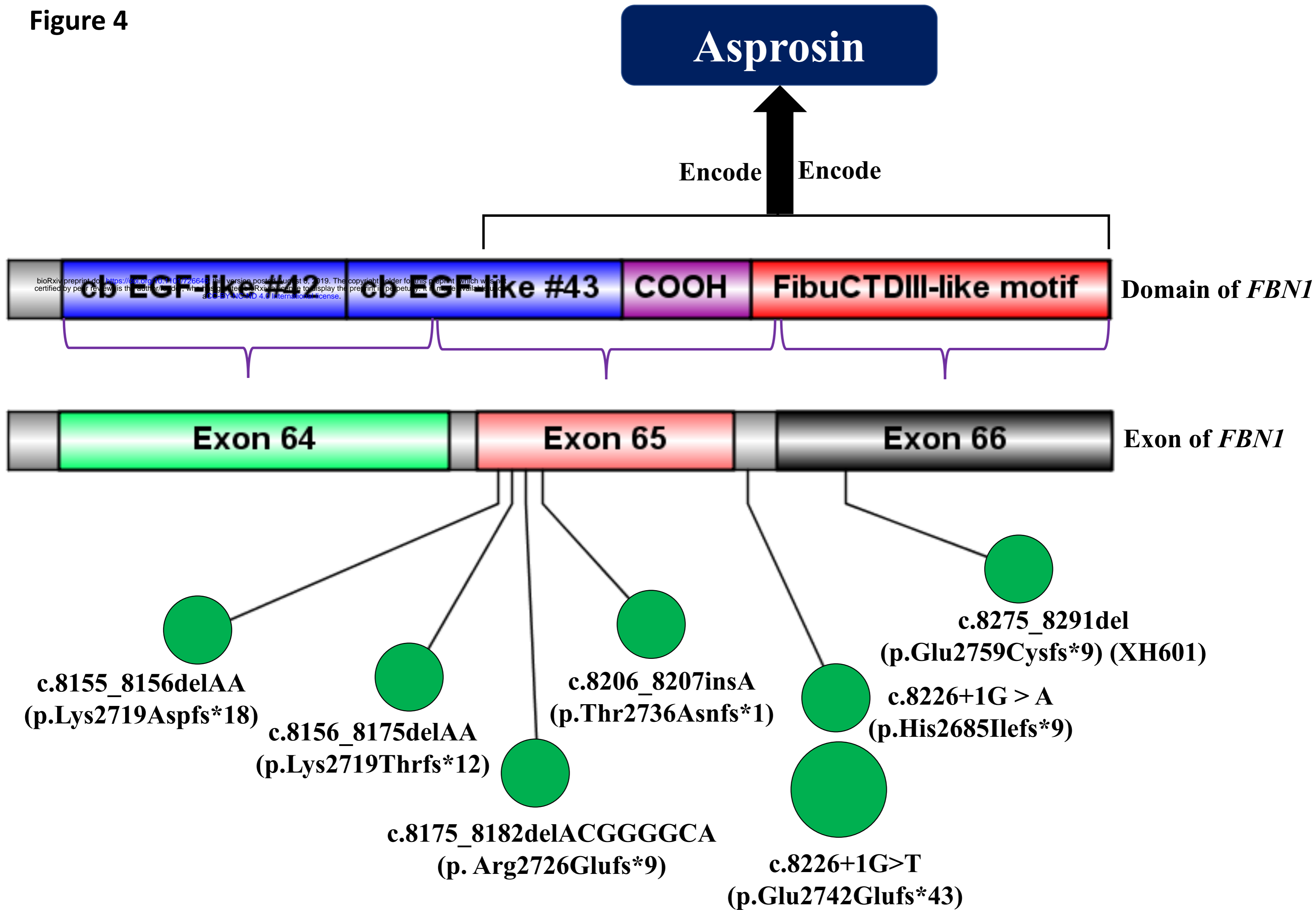
C

Figure 4

Table 1 Clinical features of Marfan syndrome patients re-evaluated for according to the revised Ghent nosology

Subject		XH253	XH474	XH601
	General patient information			
	Gender	F	F	F
	Age (years)	10	16	9
	Height (m)	1.72	1.71	1.36
	Weight (kg)	48	48	20.5
	Major Cobb angle（degrees）	43	85	117
	Major Curve type	R-T	R-T	R-T
	Curve number	3	3	2
	Curve details	UTC (38), MTC (43), LC (16)	UTC (60), MTC (85), LC (40)	MTC (117), LC (89)
	Treatment	Surgery	Surgery	Surgery
Causal *FBN1* variant				
	Nucleotide alteration	c.7785delC	c.4890_4891delGTinsTG	c.8275A8291delGAGAAGACAGCCATCTT
	Protein change	p.Tyr2596Thrfs*86	p.Gln1630_Cys1631delinsHisGly	p. Glu2759Cysfs*9
	Variant reported in MFS	None	p. Cys1631Gly	None
MFS evaluation				
	Diagnosis	MFS	MASS	Marfanoid
	Aortic root dilation (z-score)	4.5	1.3	1.6
	Ectopia lentis	A	A	A
	Systemic features score	7/20	8/20	7/20
	Wrist/thumb sign	P	P	A
	Pectus carinatum/ excavatum	A	A	A
	Hindfoot deformity	A	A	A
	Pneumothorax	A	A	A
	Dural ectasia	A	A	A
	Protrusio acetabuli	A	A	A
	UPer/lower segment	0.92	0.94	0.86
	Scoliosis or thoracolumbar kyphosis	P	P	P
	Reduced elbow extension	NA	NA	NA
	Facial features (3/5)	P	P	P
	Skin striae	A	A	A
	Myopia	-0.7 dioptries	NA	-0.4 dioptries
	Mitral valve prolapses (all types)	P	P	P

MFS denotes Marfan syndrome; MASS denotes myopia, mitral valve prolapses, borderline (Z<2) aortic root dilatation, striae, skeletal findings phenotype NA denotes not available; F denotes female; R-T denotes right thoracic spine; P denotes present; A denotes absent. UTC denotes upper thoracic curve; MTC denotes major thoracic curve; LC denotes lumbar curve.

Table 2 Clinical manifestations of previously reported and our patient XH601 with Marfanoid-progeroid-lipodystrophy (MPL) syndrome with allelic truncating mutations in *FBN1*

	Graul-Neumann et al. [2010]	Goldblatt et al. [2011]	Horn and Robinson et al. [2011]	Takenouchi et al. [2013]	Jacquinet et al. [2014]	Garg and Xing et al. [2014]		XH601 (this study)
						Patient 1	Patient 2	
Clinical characteristics								
Age (year)	27	20	3.5	10	16	23	17	9
Gender	Female	Male	Female	Female	Female	Female	Female	Female
Ancestry	Caucasian	Caucasian	Caucasian	Asian (Japanese)	Caucasian	Hispanic	Caucasian	Asian (Chinese)
Height (cm; [centile])	170	50-75	108	149	177	157.5	176	136
Weight (Kg; [centile])	39	<3	14.5	21.7	41.8	26.4	41.9	20.5
Causal *FBN1* mutation								
CDNA analysis	c.8155_8156delAA	c.8156_8175del	c.8226+1G>T, splice mutation, exon 65 skipping	c.8175_8182del8bp	c.8226+1G>A, splice mutation, exon 65 skipping and subsequent frameshift	c.8206_8027insA	c.8226+1G>T, splice mutation, exon 65 skipping	c.8275_8291del GAGAAGACAGCCATCTT
protein change	p.(Lys2719Aspfs*18)	p.(Lys2719Thrfs*12)	p.(Glu2742Glufs*43)	p.(Arg2726Glufs*9)	p.(His2685Ilefs*9)	p.(Thr2736Asnfs*1)	p.(Glu2742Glufs*43)	p.(Glu2759Cysfs*9)
Adjacent to Exon 65 in *FBN1*	Y	Y	Y	Y	Y	Y	Y	Y
Inheritance pattern	*De novo*	*De novo*	*De novo*	*De novo*	*De novo*	*De novo*	*De novo*	*De novo*
BMI (kg/m2)	13.3	NA	12.4	9.8	13.3	10.6	13.5	11.1
Body fat (%)	20.5	NA	NA	NA	NA	28.4	27.7	NA
Premature birth	Y	Y	Y	Y	Y	Y	Y	Y
Birth weight (Kg)	1.78	1.04 (<3)	1	1.427	1.72	1.19	1.17	NA
Birth length (cm)	41.5	NA	40	40	45	40	40.75	NA
Progeroid appearance	Y	Y	Y	Y	Y	Y	Y	Y
Subcutaneous fat reduction	Y	Y	Y	Y	Y	Y	Y	Y
Arm span/height	0.99	NA	NA	NA	NA	0.94	0.98	NA
Upper/lower segment	0,95	NA	NA	NA	NA	0.99	0.8	0.87
Proptosis	Y	Y	Y	Y	Y	Y	Y	Y
DPF	NA	NA	NA	NA	NA	NA	NA	Y
Myopia	Y	Y	N	Y	Severe	Y	Y	Y
Ectopia lentis	Bilateral	Bilateral	N	N	N	Left eye	N	N
High-arched palate	Y	Y	Y	NA	NA	Y	N	NA
Pectus excavatum	NA	Y	NA	Y	N	N	Y	N
scoliosis / kyphosis	Kyphosis	NA	NA	NA	N	Scoliosis	Scoliosis	Severe scoliosis
Cobb angle (degrees)	NA	NA	NA	NA	NA	NA	NA	117
Wrist sign	Y	Y	NA	NA	NA	Y	Y	Y
Thumb sign	Y	N	NA	NA	NA	Y	Y	Y
BMJD	NA	NA	NA	NA	NA	NA	NA	Y
Interosseous atrophy	NA	NA	NA	NA	NA	NA	NA	Y
Arachnodactyly	NA	NA	NA	Y	Y	NA	NA	Y
Hyperextensible digits	NA	Y	NA	Y	Y	Y	Y	Y
Pes planus /valgus	NA	Pes planus	NA	NA	Pes valgus	NA	Pes planus	NA
Easy bruisability	Y	Y	NA	NA	NA	N	N	Y
MVPS	Y	N	N	N	N	NA	Y	Y
Arrested hydrocephalus	NA	Y	Y	Y	NA	NA	NA	NA
RGC	NA	NA	NA	Hydronephrosis	N	NA	NA	N
Dural ectasia	Lumbosacral	NA	NA	Y	Y	NA	NA	N
Hypertension	NA	NA	NA	Y	NA	NA	NA	N
CHD	NA	NA	NA	NA	NA	NA	NA	Y

Abbreviations: Y, yes; N, no; NA, not available. DPF, downslanting palpebral fissures; BMJD: bilateral metacarpophalangeal joint dislocation; MVPS, mitral valve prolapse syndrome; RGC, renal/genitourinary complications. CHD, congenital hip dislocation